

Initial Simulations of Hot Vertical Displacement Events with NIMROD

C. R. Sovinec and K. J. Bunkers

University of Wisconsin-Madison

Theory and Simulation of Disruptions

July 15-16, 2015

Princeton Plasma Physics Laboratory



Objectives

Our aim is to investigate disruptive transients where vertical displacement is important. Comprehensive modeling should be able to predict:

- Development of open-field current
- Destabilization of external kink
- Forces and heat deposition on walls

Results presented here have more limited objectives:

- Demonstration of MHD-based VDE simulation with separation of Alfvén, wall, and resistive timescales
- Testing boundary conditions on \mathbf{V} and n

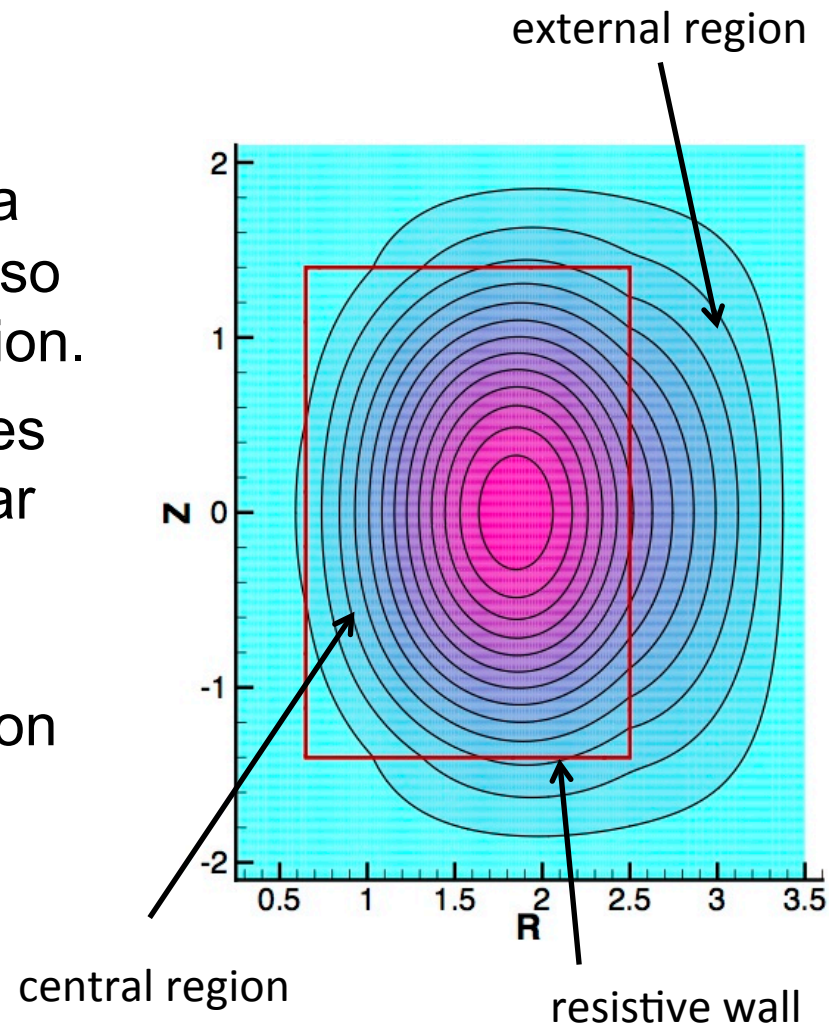
Outline

- VDE modeling with NIMROD
 - Two-region domain
 - MHD system for inner region
 - Boundary conditions
- Evolution from double-null configuration
- Single-null computations
 - Comparison of boundary conditions
 - Parallel flows
- Discussion and conclusions
- Summary of recent development
- Future work

VDE Modeling with NIMROD: The plasma region is coupled to an external vacuum region through a resistive wall.

- Plasma is modeled in the central region.
- The central region is coupled to a meshed external region that is also solved in NIMROD's representation.
- The plot on the right demonstrates poloidal flux leaking into an annular external region.
- Regions are coupled by a numerically implicit implementation of the thin-wall equation.

$$\frac{\partial \mathbf{B} \cdot \hat{\mathbf{n}}}{\partial t} = -\hat{\mathbf{n}} \cdot \nabla \times \left[\left(\frac{\eta_w}{\mu_0 \delta x} \right) \hat{\mathbf{n}} \times \delta \mathbf{B} \right]$$



Plasma evolution in the central region is modeled with a single-fluid, single-temperature system.

$$\frac{\partial n}{\partial t} + \nabla \cdot (n\mathbf{V}) = \nabla \cdot (D_n \nabla n - D_h \nabla \nabla^2 n)$$

continuity with diffusive numerical fluxes

$$mn \left(\frac{\partial}{\partial t} + \mathbf{V} \cdot \nabla \right) \mathbf{V} = \mathbf{J} \times \mathbf{B} - 2\nabla(nT) - \nabla \cdot \underline{\underline{\Pi}}$$

flow evolution

$$\frac{3}{2}n \left(\frac{\partial}{\partial t} + \mathbf{V} \cdot \nabla \right) T = -nT \nabla \cdot \mathbf{V} - \nabla \cdot \mathbf{q}$$

temperature evolution

$$\frac{\partial \mathbf{B}}{\partial t} = -\nabla \times (\eta \mathbf{J} - \mathbf{V} \times \mathbf{B}) + \kappa_b \nabla \nabla \cdot \mathbf{B}$$

Faraday's / Ohm's law with diffusive error control

$$\mu_0 \mathbf{J} = \nabla \times \mathbf{B}$$

low- ω Ampere's law

- \mathbf{B} , n , T , and \mathbf{V} are advanced in time with the NIMROD code's implicit leapfrog method [Sovinec and King, JCP **229**, 5803 (2010)].
- The diffusive control of divergence error works well with high-order elements [Sovinec, *et al.*, JCP **195**, 355 (2004)].
- The particle diffusion terms provide numerical smoothing.

The present modeling is simplified, but closure relations are important.

- Spitzer $\eta \sim T^{-3/2}$ is used throughout the central computational region that models plasma.
 - The cases shown below have $\tau_A \cong 1$ and $\eta(0) = 10^{-6}$. With $a \cong 0.75$, $S(0) \cong 5 \times 10^5$. T profiles vary by 10^4 .
 - Number density profiles vary by 10.
 - Large resistivity outside the plasma part of the central region keeps current density negligible.
- Thermal conduction is anisotropic, $\mathbf{q} = -n \left[\chi_{\parallel} \hat{\mathbf{b}}\hat{\mathbf{b}} + \chi_{\perp} (\mathbf{I} - \hat{\mathbf{b}}\hat{\mathbf{b}}) \right] \cdot \nabla T$, with $\chi_{\parallel} = 5 \times 10^{-2}$ and $\chi_{\perp} = 5 \times 10^{-6}$.
- Viscous stress is isotropic, $\underline{\Pi} = -nm_i \nu_{iso} \left(\nabla \mathbf{V} + \nabla \mathbf{V}^T - \frac{2}{3} \underline{\mathbf{I}} \nabla \cdot \mathbf{V} \right)$, with $\nu_{iso} = 5 \times 10^{-5}$.
- Sources and heating are not included in these computations.

Computation in the outer vacuum region approximates magnetostatic responses.

- The standard approach uses a magnetic potential.

$$\mathbf{B} = \nabla\chi, \quad \nabla^2\chi = 0 \text{ in } R_{out}, \quad \hat{\mathbf{n}} \cdot \nabla\chi = B_{n_{out}} \text{ on } \partial R_{out}$$

where χ may be multi-valued in regions that are not topologically spherical.

- A given static solution can also be found as the long-time response to a diffusion problem. $(\tau_{wall} \gg L^2/\eta_{out})$

$$\frac{\partial}{\partial t}\mathbf{B} = \eta_{out}\nabla^2\mathbf{B} \quad \text{subject to} \quad \hat{\mathbf{n}} \cdot \mathbf{B} = B_{n_{out}} \text{ on } \partial R_{out}.$$

- This is convenient in NIMROD, which solves the plasma response in terms of \mathbf{B} .
- Induction from changes in I_p appear through surface- \mathbf{E}_{tang} .
- Outer-region computations are fast relative to the plasma update.

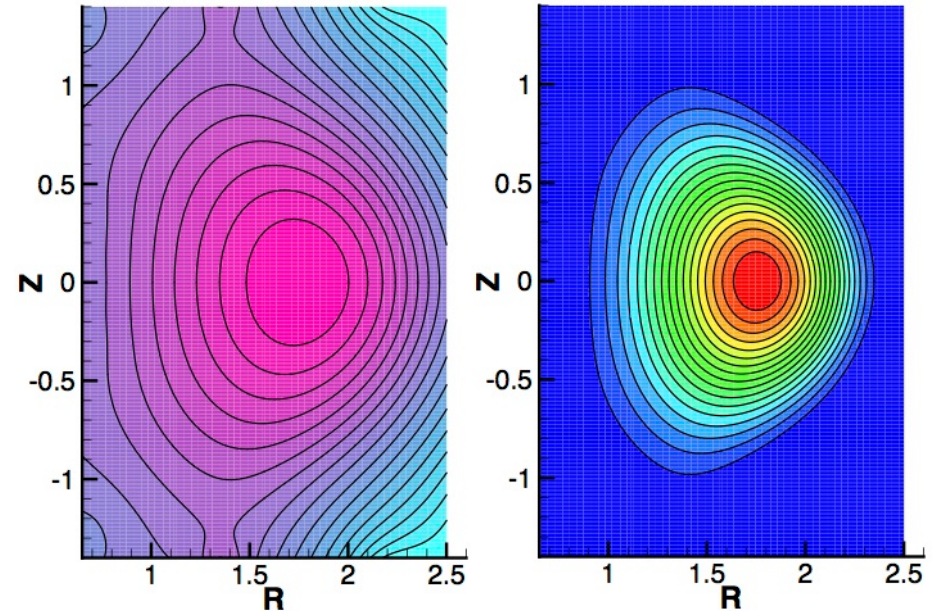
Boundary conditions on \mathbf{B} are set at the outer boundary, while conditions on n , T , and \mathbf{V} are set along the perimeter of the central region.

- Standard conditions for NIMROD simulations with thermal conduction and particle diffusion are:
 - n and T remain fixed at their initial low values.
 - All components of flow are zero, $\mathbf{V} = 0$.
- Conditions based on magnetic drift have been implemented:
 - Flow drifts out, based on the resistive-wall \mathbf{E} .

$$\hat{\mathbf{n}} \cdot \mathbf{V} = \hat{\mathbf{n}} \cdot \frac{1}{B^2} \mathbf{E}_w \times \mathbf{B} \text{ , where } \mathbf{E}_w = \left(\frac{\eta_w}{\mu_0 \delta x} \right) \hat{\mathbf{n}} \times \delta \mathbf{B}$$
 - T remains fixed at its initial value.
 - n is either fixed *or* advects into the resistive wall, $\hat{\mathbf{n}} \cdot \Gamma = \hat{\mathbf{n}} \cdot (n\mathbf{V})$, which has been implemented with the explicit (old) n at each step.
- Along the outer boundary, $\hat{\mathbf{n}} \times \mathbf{E} = \mathbf{0}$, so $\hat{\mathbf{n}} \cdot \mathbf{B}$ is fixed.

Double-null case: This configuration models vertical instability from loss of divertor-coil current.

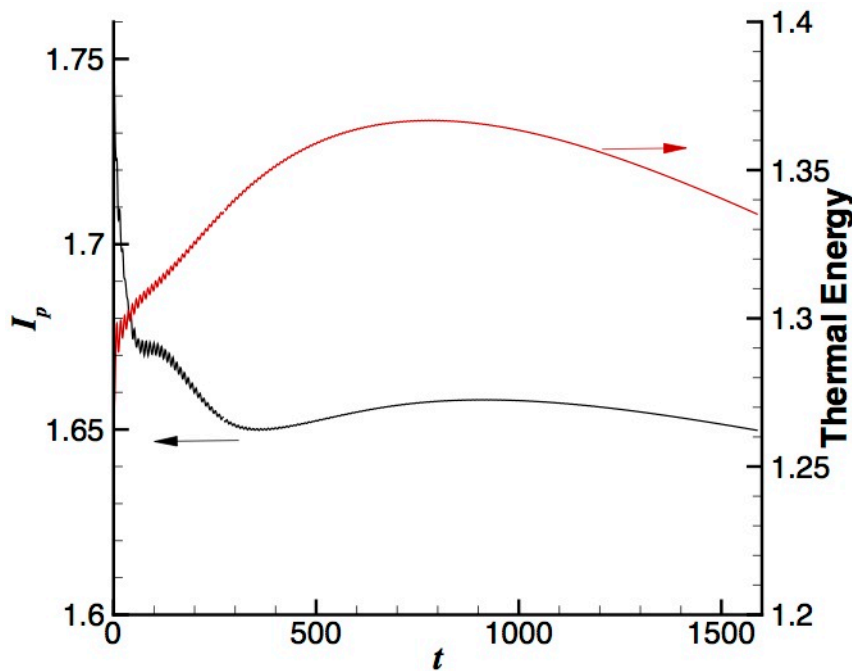
- The initial state is from a free-boundary Grad-Shafranov computation with NIMEQ [Howell and Sovinec, CPC 185, 1415 (2014)].
- $P(\psi)$ and $F(\psi)$ profiles are simple quadratic and linear functions, respectively, but values are based on DIII-D with F nearly uniform and $\beta(0)=8\%$.
- The MHD computations have n fixed and drift conditions on \mathbf{V} along the inner-region boundary.
- The resistive wall sets the time-scale for vertical displacement.
 - τ_r for the initial profile is of order 10^5 .
 - With $\eta_w/\mu_0\delta x = 10^{-3}$ and $a \sim 1$, $\tau_w \sim 10^3$.



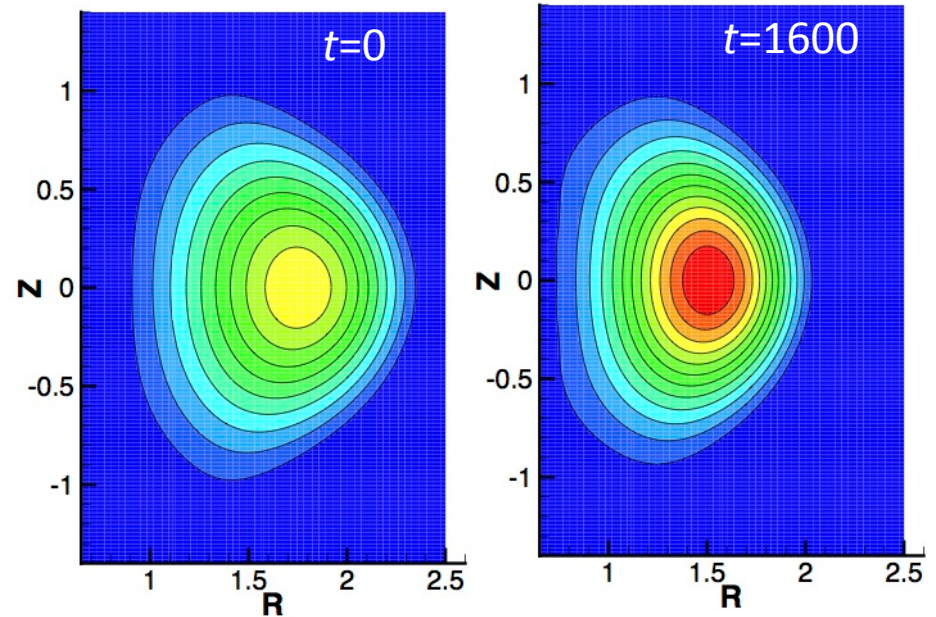
Inner-region poloidal flux (left) and pressure (right) from equilibrium computation.

The simulated tokamak remains vertically centered in a “control” case.

- Here, all coil currents are fixed.
- There is a transient, possibly from poor initialization of secular flux in the outer region, and the net motion is radial.



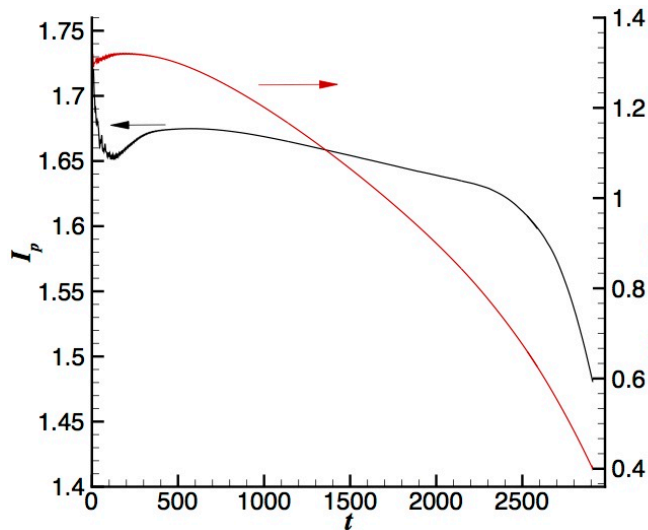
Plasma current drops by 6% over the first $300 \tau_A$, and internal energy increases over the first $700 \tau_A$, as the discharge moves radially inward.



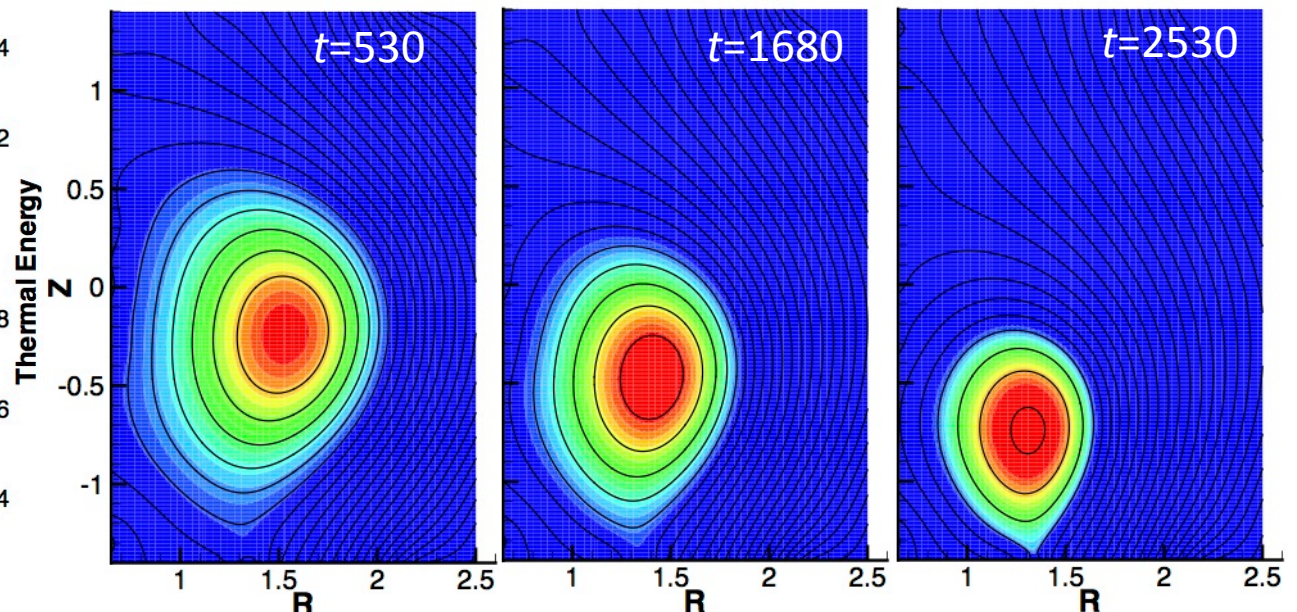
Contours of initial (left) and final (right) pressure show radial motion and compression.

Turning the upper divertor coil off at $t = 0$ initiates a vertical instability that develops on the wall timescale.

- The external magnetic perturbation diffuses through the wall.
- Radial motion and initial evolution in I_p resemble the control case.
- Vertical motion and loss of thermal energy are consequences of the magnetic perturbation.
- The tokamak remains hot while in contact with the wall.



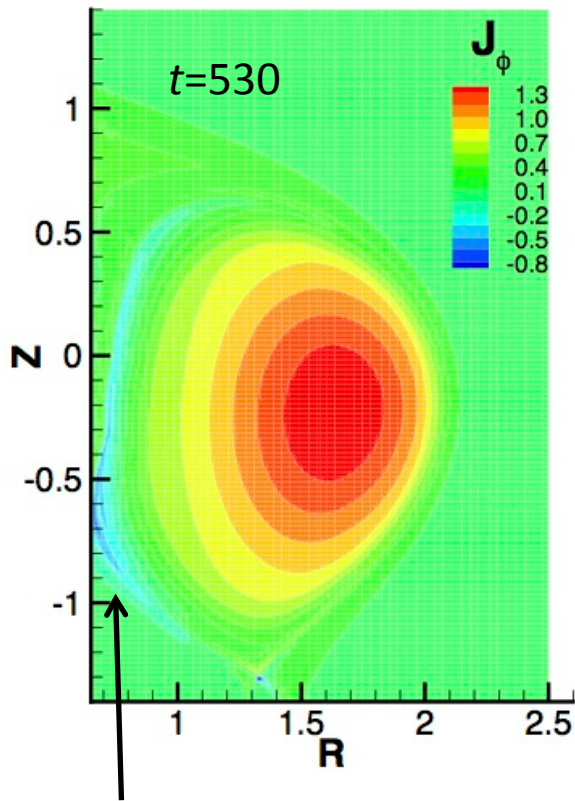
Thermal energy (red) decreases more rapidly than current.



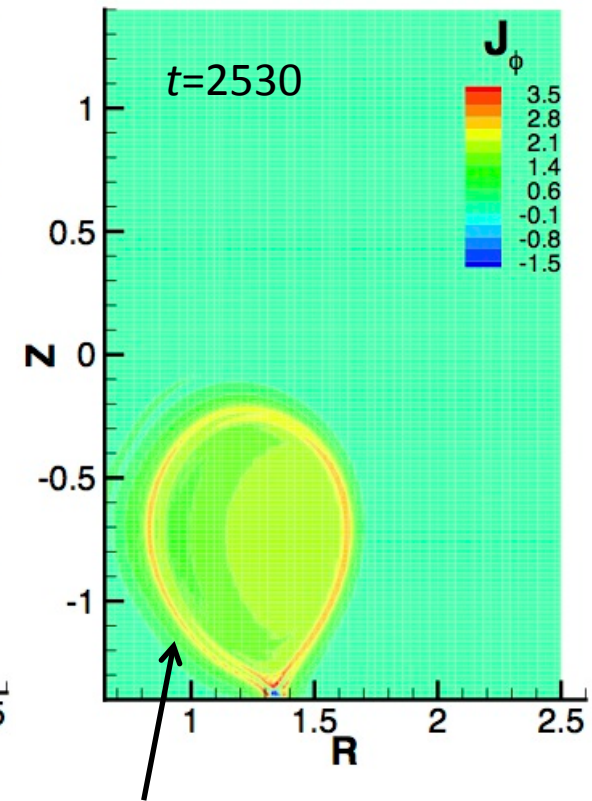
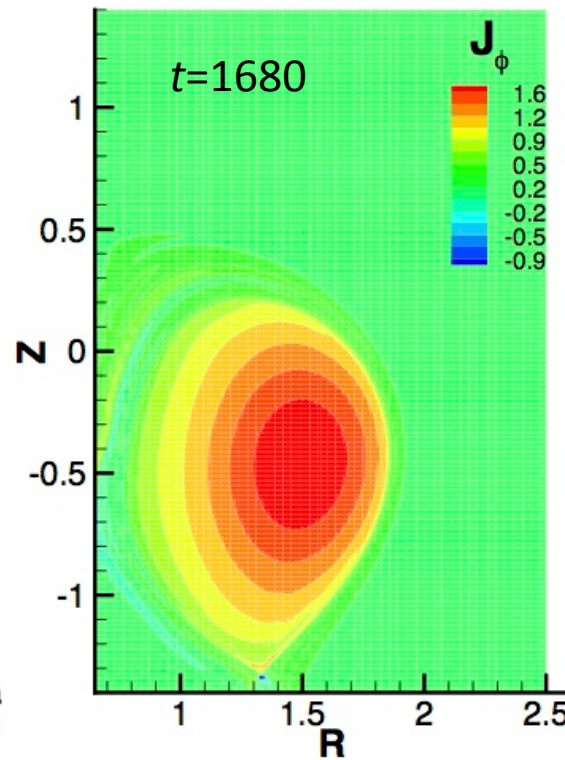
Vertical displacement is evident in contours of poloidal flux (black) overlaid on contours of pressure (same scale for all times).

The current density profile evolves significantly while I_p changes slowly.

- The magnitude of J_ϕ increases over time.
- A thin halo of positive (axisymmetric) toroidal current supports pressure and RB_ϕ late in time.



Reversed current develops during early dynamics.



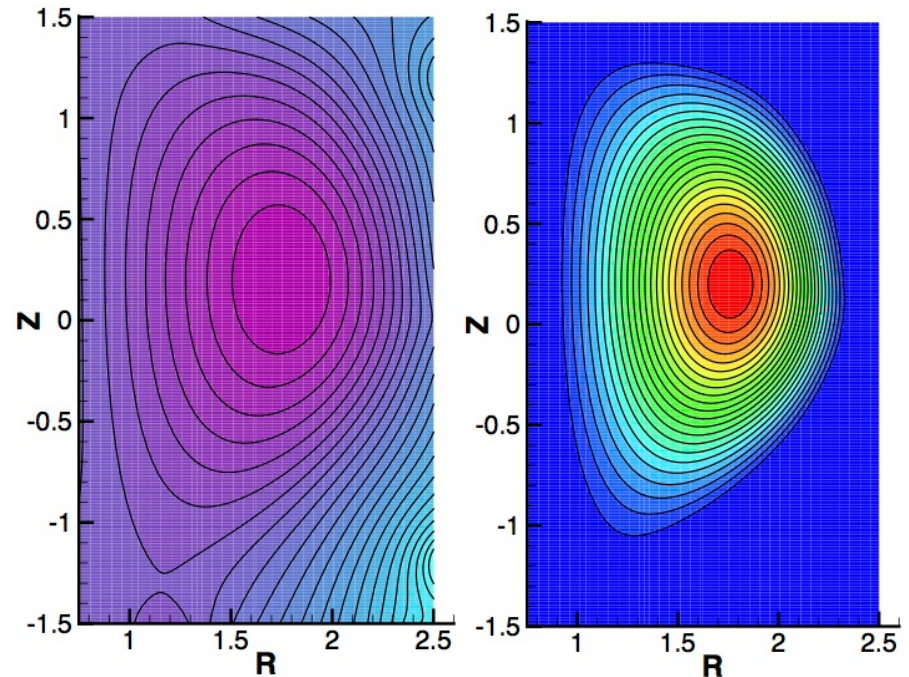
Halo current that supports equilibrium is evident.

Single-null cases: We compare boundary conditions on n and \mathbf{V} in this configuration.

- Initial conditions are taken from a fixed-boundary Grad-Shafranov computation.
- External region has a horseshoe shape.
- External coil currents are fixed.
- Decay of initial eddy currents allows axisymmetric displacement.
- Along the resistive wall, computations use either $\mathbf{V} = 0$ or the drift condition,

$$\hat{\mathbf{n}} \cdot \mathbf{V} = \hat{\mathbf{n}} \cdot \frac{1}{B^2} \mathbf{E}_w \times \mathbf{B}$$

- Boundary conditions on n are either inhomogeneous Dirichlet or as governed by advective flux.



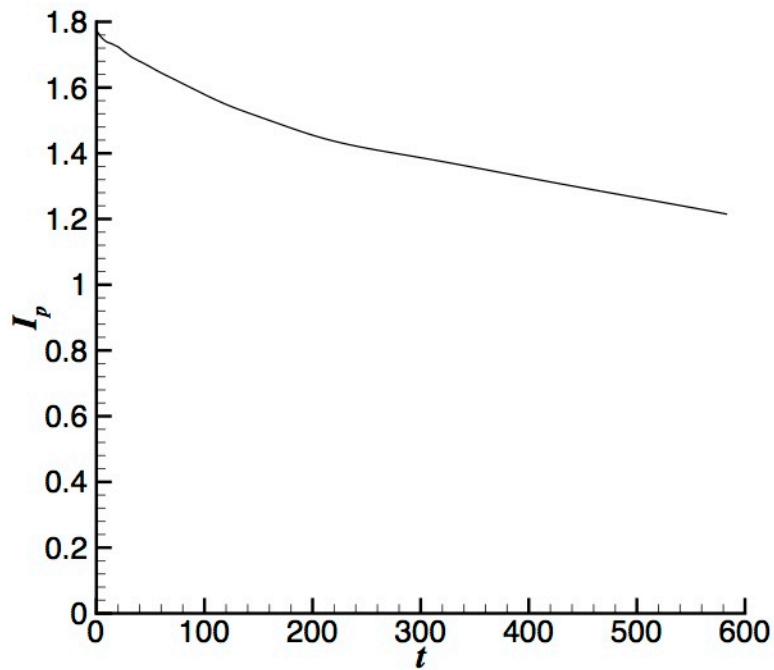
Poloidal flux (left) and pressure (right) for the initial conditions.

As in the previous cases,

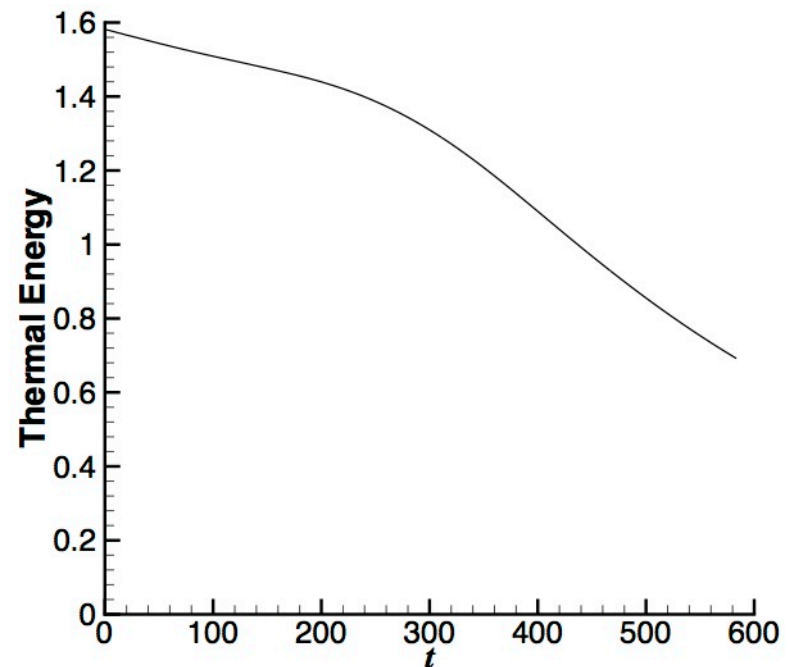
- τ_r for the initial profile is of order 10^5 .
- With $\eta_w/\mu_0 \delta x = 10^{-3}$ and $a \sim 1$, $\tau_w \sim 10^3$.

Decay of the initial eddy currents leads to slow axisymmetric instability.

- Over $400 \tau_A$, plasma current (I_p) decreases by 25% and thermal energy decreases by 31%.



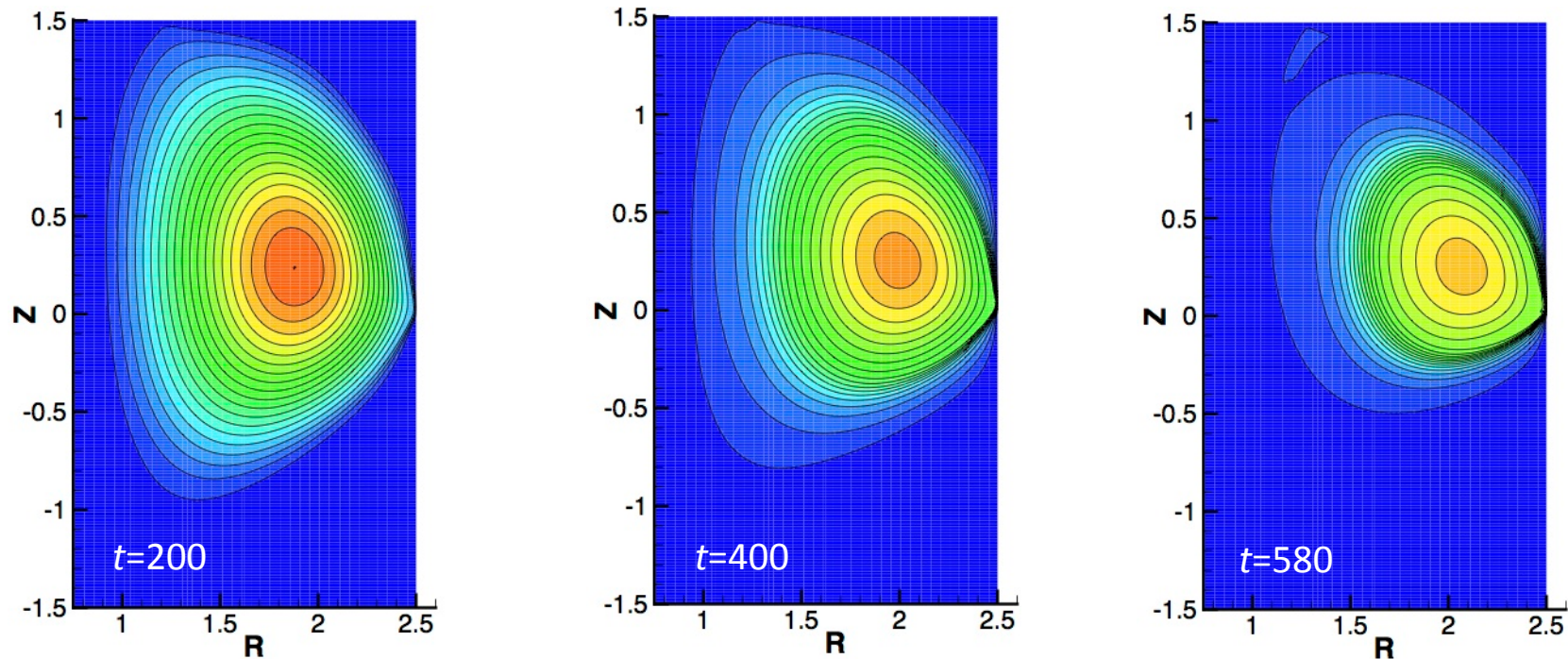
Plasma current evolution through $600 \tau_A$.



Internal energy decays faster than current after $300 \tau_A$ due to thermal transport from outer surfaces.

Displacement from the decay of eddy currents is primarily radial in these cases.

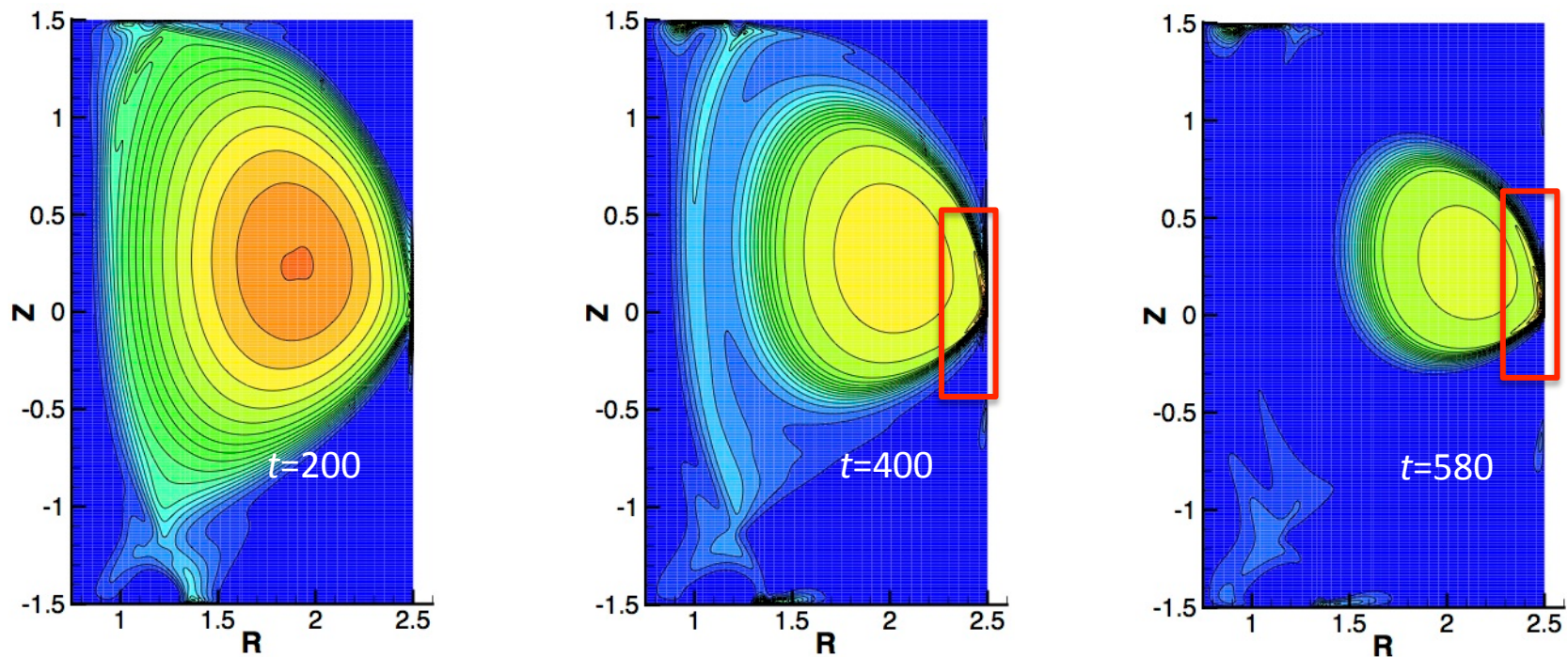
- This configuration has an attracting coil at $R=2.6$, $Z=0$ (triangularity) between vertical-field coils at $Z=\pm 1.2$.
- Edge plasma cools through contact with the wall as the configuration changes from diverted to limited.



Contours of temperature (same scale for all times) show that confinement remains intact for a central core region.

With the Dirichlet boundary condition on n , diffusion allows mass to escape.

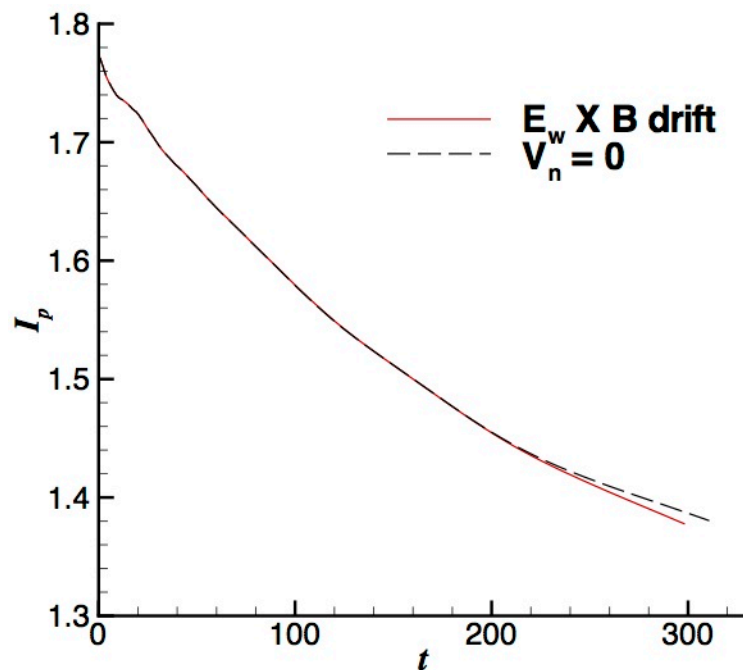
- Mass piles-up in layers near the points of contact.
- Outward mass flux results from $\hat{\mathbf{n}} \cdot \Gamma_D = -\hat{\mathbf{n}} \cdot (D_n \nabla n - D_h \nabla \nabla^2 n)$ along the surface.
- The scale of the layers is affected by D_n and D_h values (5×10^{-6} and 1×10^{-10} , respectively).



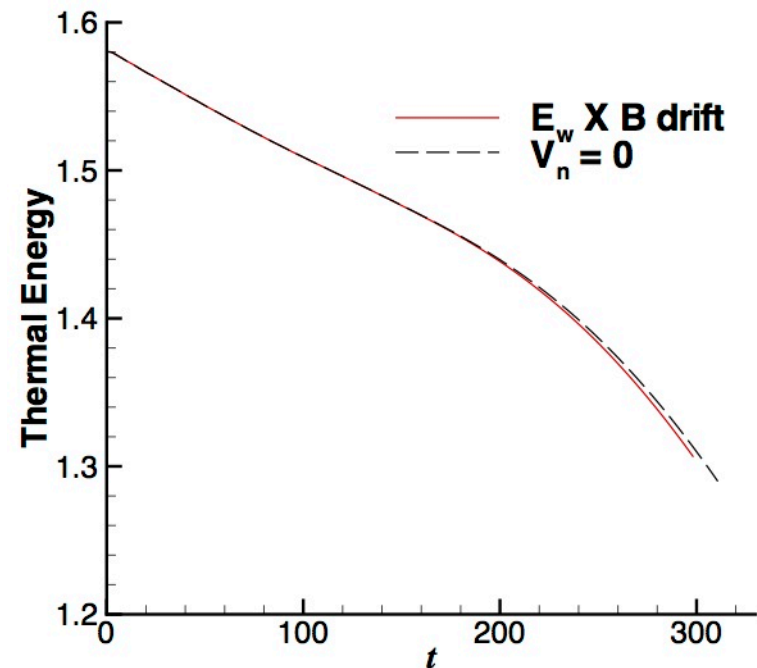
Contours of particle density show a thin pile (marked in red) near the contact point.

The evolution of current and thermal energy is essentially unchanged when the normal component of flow is set by $\mathbf{E}_w \times \mathbf{B}$ drift.

- The comparison here is through $300 \tau_A$.
- Mass flow through the boundary is set by $\hat{\mathbf{n}} \cdot \Gamma = \hat{\mathbf{n}} \cdot (n\mathbf{V})$ in the computation with the drift-flow condition.

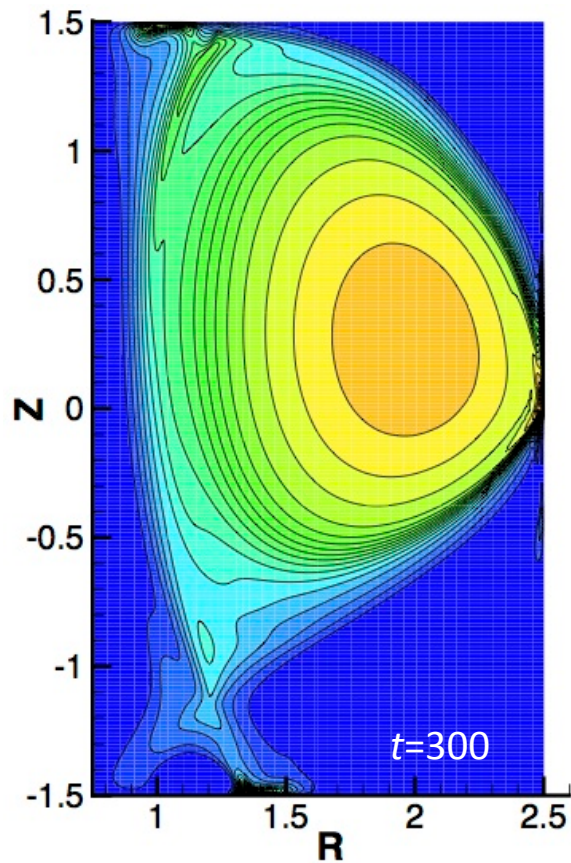


Plasma current comparison through $300 \tau_A$.

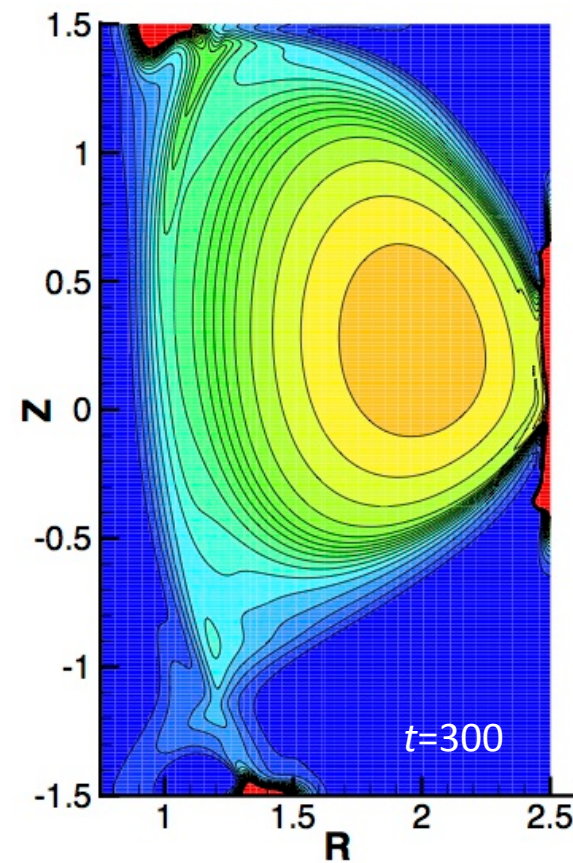


Internal energy again decays faster than current near the end of this period.

Accumulation of mass along the surface is larger with the advective mass flux condition, however.



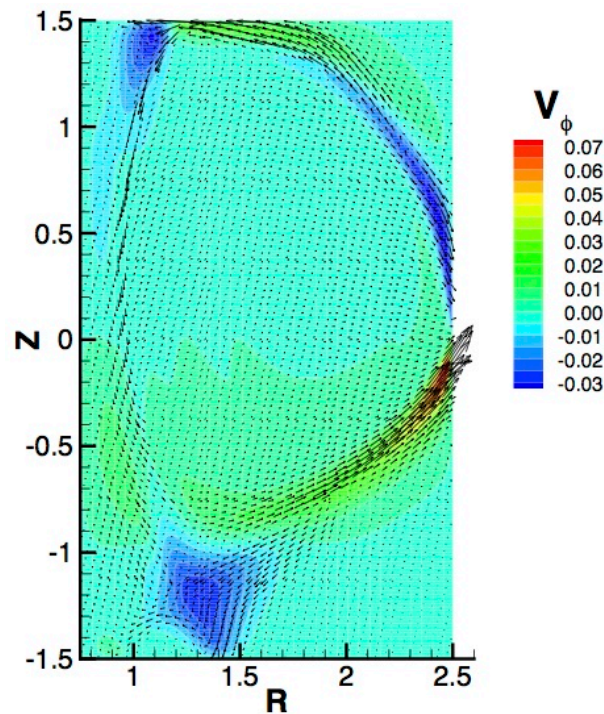
Mass density at $300 \tau_A$ with $V_n=0$ and diffusive particle flux along surface.



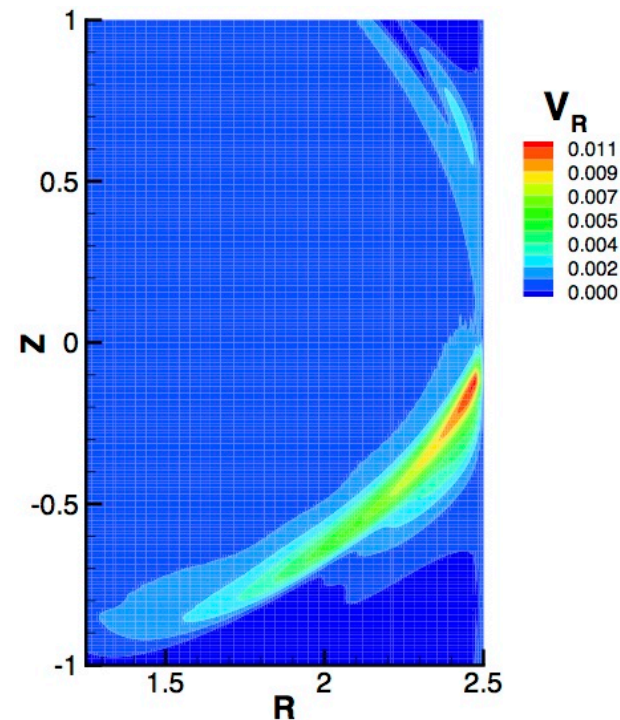
Mass density at $300 \tau_A$ with drift outflow and advective particle flux (no diffusive flux) along the surface.

The flow velocity that sends mass to the wall is larger than the $\mathbf{E}_w \times \mathbf{B}$ drift, hence the accumulation of mass.

- Along the outer wall, $\delta B \approx 0.1$ and $B_\phi = 1$, so the normal component of the $\mathbf{E}_w \times \mathbf{B}$ drift is approximately 10^{-4} .
- V_R exceeds 10^{-2} , 100 times larger, so the $\mathbf{E}_w \times \mathbf{B}$ drift is negligible.
- $B_\phi \approx 5B_{pol}$ near the outer wall, and with $V_\phi = 0.07$, \mathbf{V} is largely parallel to \mathbf{B} .

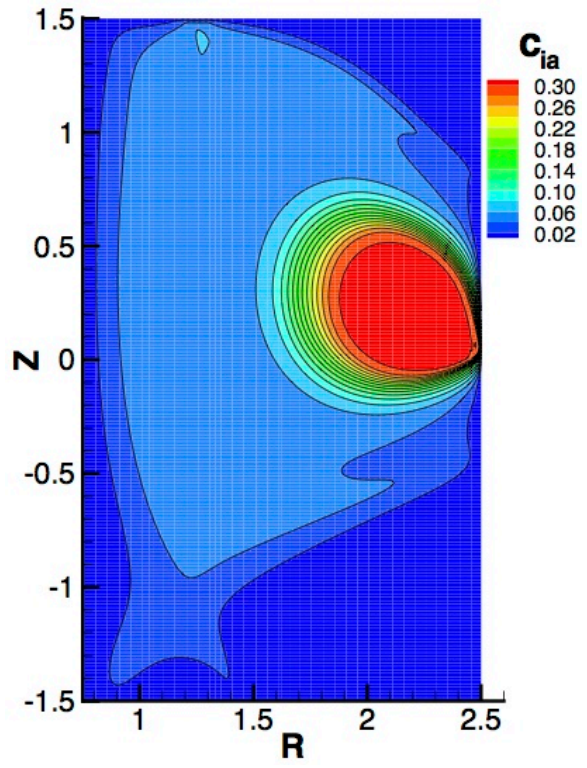


Contours of V_ϕ with poloidal vector components at $300 \tau_A$.

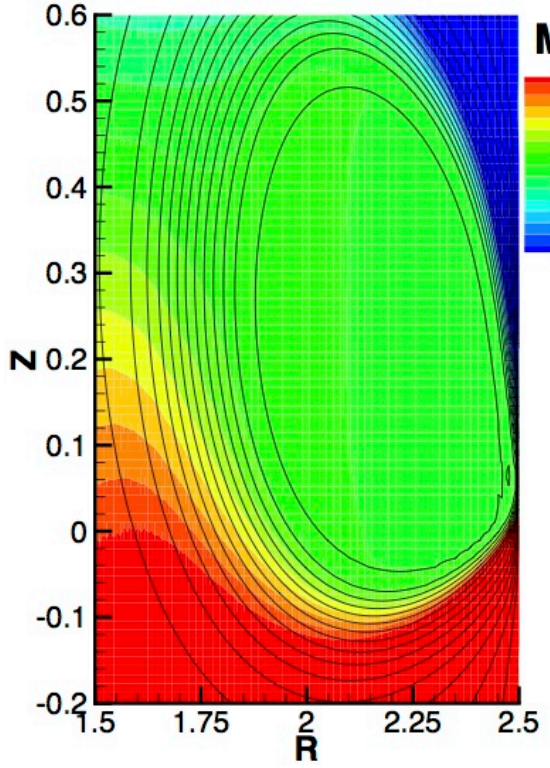


Radial component of \mathbf{V} near contact point.

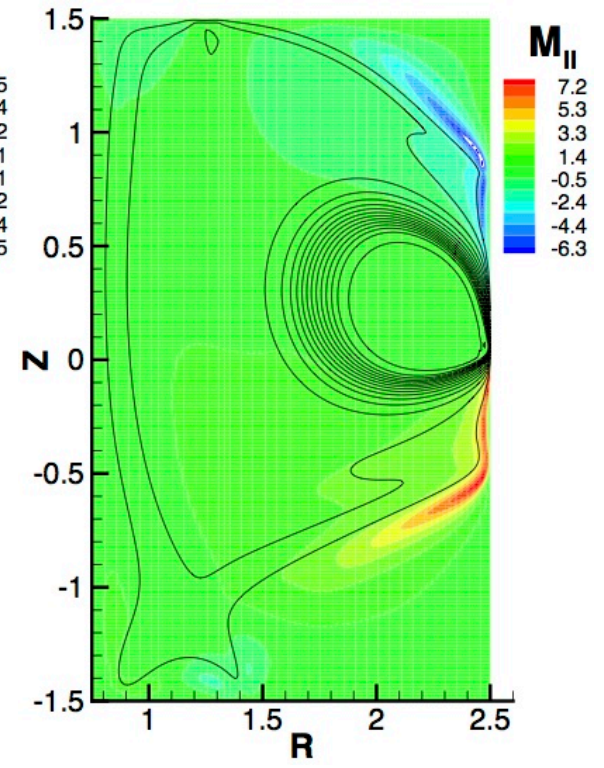
Parallel flow along open surfaces is accelerated by thermal pressure.



Contours ion-acoustic speed at $900 \tau_A$ show a confined region and a remnant.



Near-sonic parallel flow develops around confined region; color= $M_{||}$, lines= c_{ia} .



Low-density flow from the remnant becomes supersonic when cooled.

- Plasma inertia is important for the open-field parallel flow.
- A parameter scan (not displayed) finds that flows in the remnant region are sensitive to thermal conductivity and viscosity.

Discussion and Conclusions

- Results with $\mathbf{E}_w \times \mathbf{B}$ drift conditions at the wall and advective particle flux are similar to results with $V_n=0$ and Dirichlet conditions on n .
 - The extent of mass accumulation differs, and the diffusive flux case allows greater loss of mass.
 - Near-sonic parallel flows result from thermal effects.
 - The boundary conditions on flow do not impede magnetic diffusion through the wall. [Also see Strauss, PoP **21**, 032506 (2014).]
- The computations also illustrate the applicability of implicit methods to slowly evolving states.
 - Timesteps in the computations are of order $0.1-1 \tau_A$, approximately 5000 times larger than explicit.
 - They 1-10 times larger than the flow-CFL condition.

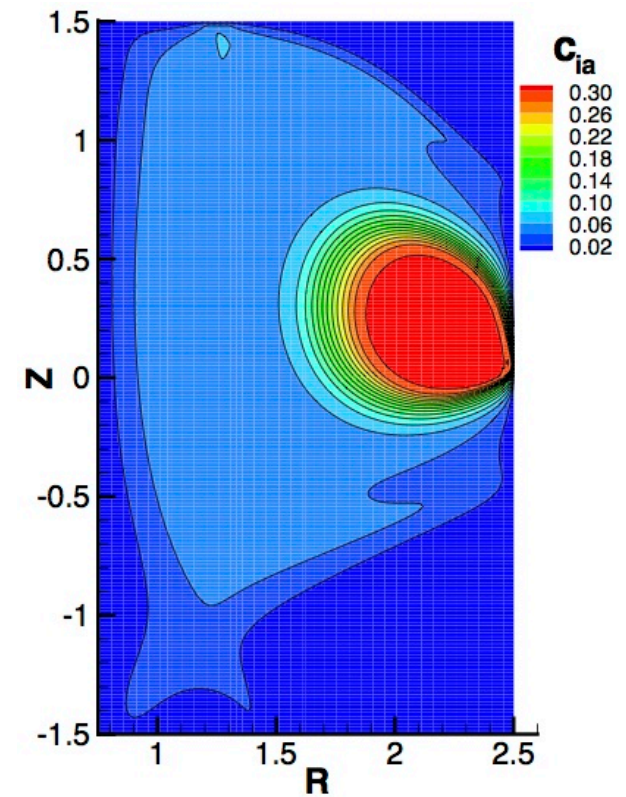
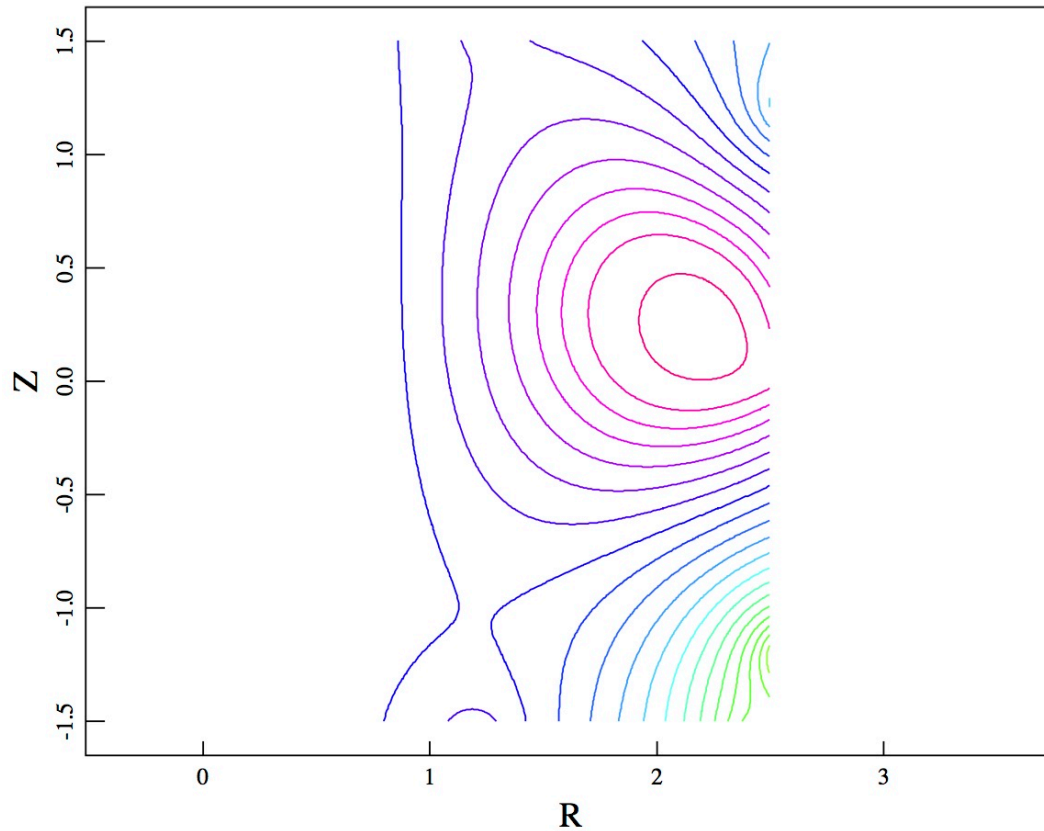
Summary of Recent Development

- Free-boundary Grad-Shafranov solves in NIMEQ
- Parallel computation for multi-region problems with implicit coupling through the resistive wall
- Annular mesh assembly for outer regions

Next Steps

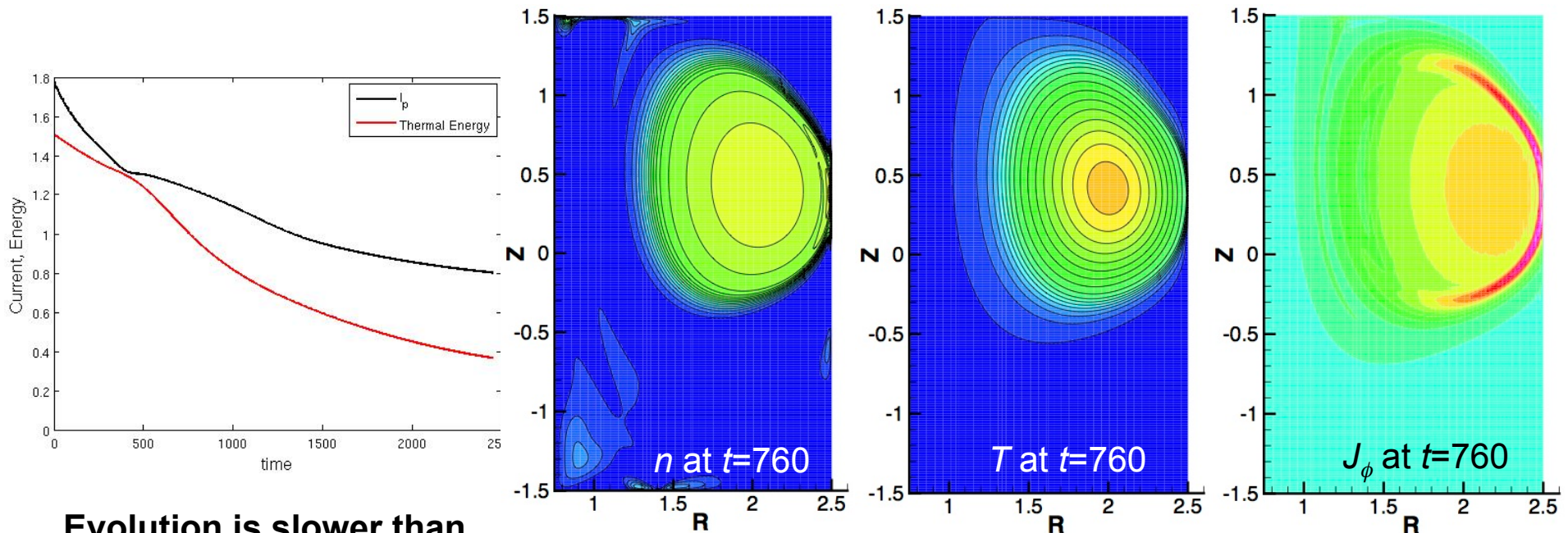
- Improved outer-region initialization of secular flux.
- Evaluate stresses on the wall.
- Use more realistic closures for thermal conductivity and viscosity.
- Include sources: heating, current drive, particle source.
- Investigate coupled VDE/kink dynamics in three dimensions.
- Implement boundary relations that model sheath conditions.

The low-temperature remnant region is shaped by poloidal flux, hence anisotropic thermal conduction.



Another case does not use the outboard shaping coil, and the subsequent evolution is slower.

- The drift condition is used on V_n , but the Dirichlet condition is used for n .
- The upper limit on η is 1, and $\eta(T)$ varies by 10^6 over the central region.



Evolution is slower than cases with the shaping coil. I_p is just below 50% after nearly $2500 \tau_A$.

Profiles of density and temperature show greater vertical displacement.

Contours of J_ϕ show a sheet of positive current.

- This computation uses larger numerical time-steps of $\sim 1.7 \tau_A$ on average.